4 Oxide Heterostructure Project

– Observation and control of novel quantum phenomena in superstructures of strongly correlated oxides –

Project Leader: Hiroshi KUMIGASHIRA

4-1 Introduction

The goal of this project is to design novel physical properties appearing at the heterointerface of strongly correlated oxides. The physical properties arise from strong mutual coupling among the spin, charge, and orbital degrees of freedom in the interface region between two different oxides [1]. In order to control such properties, it is necessary to clarify the interfacial electronic, magnetic, and orbital structures. We are therefore using synchrotron radiation spectroscopic techniques having elemental selectivity to probe these structures in the nm-scale at the oxide heterointerface. For example, the electronic structure at the interface is determined by photoemission spectroscopy (PES) and X-ray absorption spectroscopy (XAS), the magnetic structure by magnetic circular dichroism of XAS, and the orbital structure by linear dichroism of XAS. We aim to design and create novel quantum materials by optimally combining sophisticated oxide growth techniques using laser molecular beam epitaxy (MBE) and advanced analysis techniques using quantum beams.

4-2 Construction of new beamline for surface and interface studies of oxide superstructures

We have designed and constructed a new undulator beamline MUSASHI (Multiple Undulator beamline for Spectroscopic Analysis on Surface and HeteroInterface) at the BL-2 section of the PF-ring (Fig. 1). This new beamline has two types of undulator in tandem alignment; one is designed for the vacuum ultraviolet (VUV) region (30–300 eV), and the other for the soft X-ray (SX) region (250–2000 eV). Consequently, relatively wide energy-range light while maintaining both high brilliance and high energy resolution will be available in this beamline by the combination of the two undulators and a variable-included-angle varied-line-spacing plane-grating (VLSPG) monochromator. Moreover, an additional double-crystal monochromator is built into this branch beamline to have the energy range of 2000–4000 eV available using the wiggler mode of the SX undulator. Our developed system "*in-situ* photoelectron spectrometer – laser MBE" will be installed at the new beamline BL-2A as an endstation (Fig. 2).

Previously, we had mainly used the *in-situ* PES – laser MBE system either at BL-28 for angle-

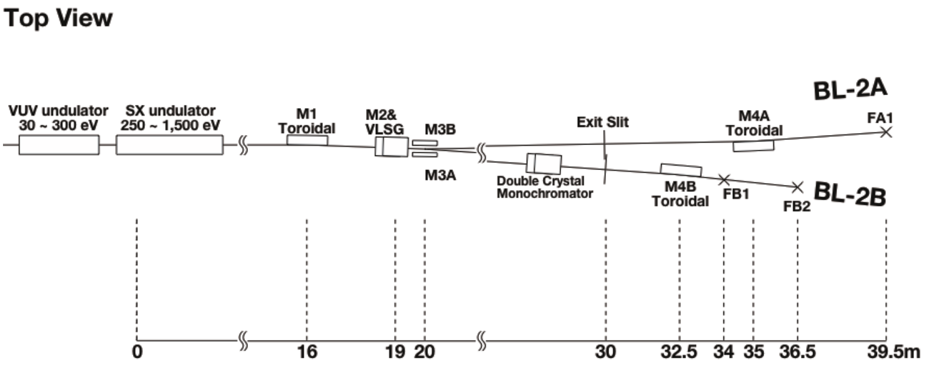

Fig. 1: Layout of new BL-2 "MUSASHI".

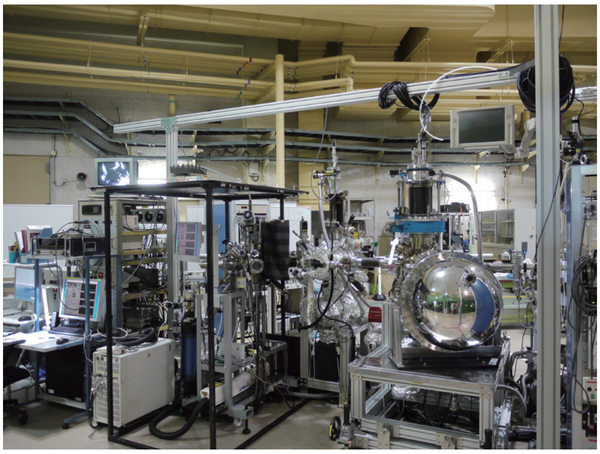

Fig. 2: Photo of the developed in-situ ARPES – Laser MBE system installed at the MUSASHI beamline.

resolved photoemission spectroscopy (ARPES) in the VUV region or at BL-2C for photoemission spectroscopy and X-ray absorption spectroscopy in the SX region. However, at the new BL-2A, we will perform both VUV and SX spectroscopic measurements at the same time, for the same grown sample, with the same experimental setup. Such a feature guarantees the quality of the experimental data, and offers numerous benefits to the field of surface science: the newly developed system enables us to obtain complete information on the electronic and chemical structures of samples grown by laser MBE with high reproductivity. For example, the chemical states and band lineup of heterostructures are characterized by core-level spectroscopy using SX light, confirming the quality of the heterostructures, and then their quantum well (QW) states are investigated by ARPES using VUV light. The beamline "MUSASHI" will be available at the end of 2014.

4-3 Science topic: Determination of the surface and interface phase shifts in metallic quantum well structures of perovskite oxides

Quantum well (QW) states have greatly contributed to the development of both fundamental physics and electronic devices used for modern information technology [1-3]. Recently, metallic QW states were clearly observed for strongly correlated oxides by ARPES: $SrVO_3$ (SVO) ultrathin films [4] as well as cleaved $SrTiO_3$ (STO) and $KTaO_3$ surfaces [5-7]. Such QW structures are relevant to understanding two-dimensional quantum confinement (phenomena) in strongly correlated oxides, which have attracted considerable attention for their potential use in controlling the novel functionalities of strongly correlated oxides using artificial structures.

In order to design the functionalities of the oxide QW structures, it is desirable to obtain knowledge of the complex interactions of the confined strongly correlated electrons at the boundaries, especially the phase shift (reflection) of the electrons at the surface and the interface. However, unfortunately, the phase shifts at the two boundaries cannot be extracted separately because one obtains information as a "total phase shift" term of Φ, which is defined as the sum of the phase shifts at the surface ($\Phi_{surf.}$) and the interface ($\Phi_{interf.}$) in the quantization condition for a numerical formula [1-3]. Therefore, the phase shifts at the two boundaries have been treated as the fitting parameters to describe the QW states, although the phase shift is an essential term to discuss the confinement condition in metallic QW structures.

In order to overcome these difficulties, we propose a method of analysis to experimentally determine the phase shifts at the two boundaries using the "asymmetric and symmetric" QW structures, as shown in Fig. 3. These QW structures consist of isostructural perovskite oxides with a chemical formula of ABO_3. The symmetric $A'B'O_3/ABO_3/A'B'O_3$ QW structures, where electrons are geometrically confined inside the ABO_3 layers, have the same boundaries as the $ABO_3/A'B'O_3$ interfaces. Thus the total phase shift of this symmetric QW structure is twice the phase shift at the ABO3/ $A'B'O_3$ interface ($\Phi^{\text{Sym.}} = 2\Phi_{interf.}$). Meanwhile, the total phase shift of the asymmetric QW structure (vacuum/ABO3/A'B'O3) is obtained as the sum of the phase shifts at the ABO3 surface and the ABO3/ A'B'O3 interface ($\Phi^{\text{Asym.}} = \Phi_{surf.} + \Phi_{interf.}$). As a result,

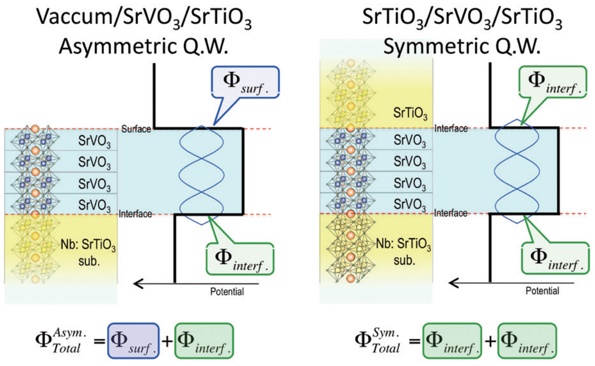

Fig. 3: Schematics of the $SrTiO_3/SrVO_3/SrTiO_3$ "symmetric" and vacuum/$SrVO_3/SrTiO_3$ "asymmetric" QW structures.

the phase shifts at the surface and the interface are separately determined by solving the simple simultaneous equations.

Using the metallic QW structures composed of the conductive oxide SVO and the oxide semiconductor STO, we successfully determined the phase shift at the surface (vacuum/SVO) and the interface (STO/SVO) by analyzing an SVO-layer thickness series of ARPES spectra [8]. Figure 4 shows the ARPES spectra taken at the Γ point as a function of SVO film thickness with and without an STO overlayer. The former corresponds to the symmetric QW structure of STO/SVO/STO, whereas the latter is the asymmetric QW structure of vacuum/SVO/STO. Regardless of the presence or absence of the STO overlayer, several peaks derived from the QW states were clearly observed in the ARPES spectra. Because STO is an *n*-type semiconductor with a band gap of 3.2 eV, an STO overlayer does not mask the QW states derived from the V 3*d* states of the buried SVO layers. Thus we address the buried QW states by ARPES. At first glance, there seems to be no significant change in both the ARPES spectra; the spectral line shapes are similar to each other, and the number of peaks is the same in the ARPES spectra for the same SVO film thickness. However, a closer look reveals that the peak positions of the quantized states show slight differences between the two QW structures. The quantized states located in the vicinity of the Fermi level (E_F) are slightly shifted toward a higher binding energy in the “symmetric” QW structure of STO/SVO/STO, whereas the quantized states near the bottom of the V 3*d* conduction bands shift in the opposite direction.

In order to investigate the differences in the quantized states between the two kinds of QW structures more clearly, we plot the peak positions as a function of SVO film thickness in Fig. 5. For both of the QW structures, the quantized states are finally saturated at the binding energy of ~500 meV, where the bottom of the bulk V 3*d* conduction bands in SVO is located [4]. As expected from Fig. 4, the quantized states located in the lower binding energy region exhibit differences in their peak positions between the two QW structures. Considering the structural difference in these QW structures, the differences in peak positions should reflect the degree of the quantum confinement at the surface and the interface, which is represented by the total phase shift in the phase shift quantization rule [1-3].

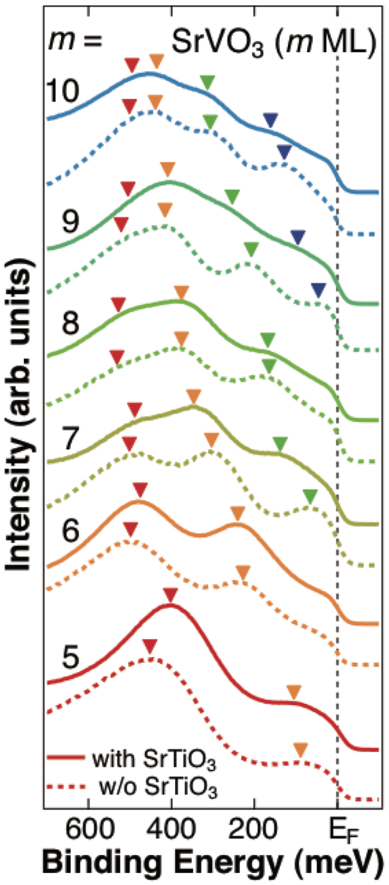

Fig. 4: Thickness-dependent ARPES spectra of $SrVO_3$ ultrathin films taken at the Γ point with (solid lines) and without (dashed lines) a $SrTiO_3$ overlayer. The filled triangles indicate the peak positions in the ARPES spectra.

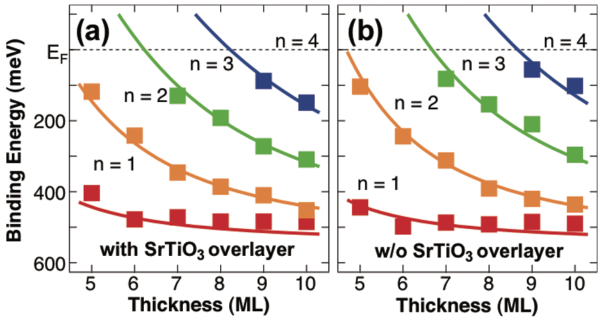

Fig. 5: Structure plot of $SrVO_3$ ultrathin films (a) with and (b) without a $SrTiO_3$ overlayer. The marker colors correspond to those of the triangles in Fig. 4. The markers and solid lines are the experimental data and simulated results based on the phase shift quantization rule, respectively.

To estimate the total phase shifts for both of the QW structures, we simulated the structure plots by changing only the total phase shift, while other parameters were fixed [4,8]. These results are superimposed on the solid lines in Figs. 5(a) and 5(b) for the symmetric and asymmetric QW structures, respectively. The simulated results

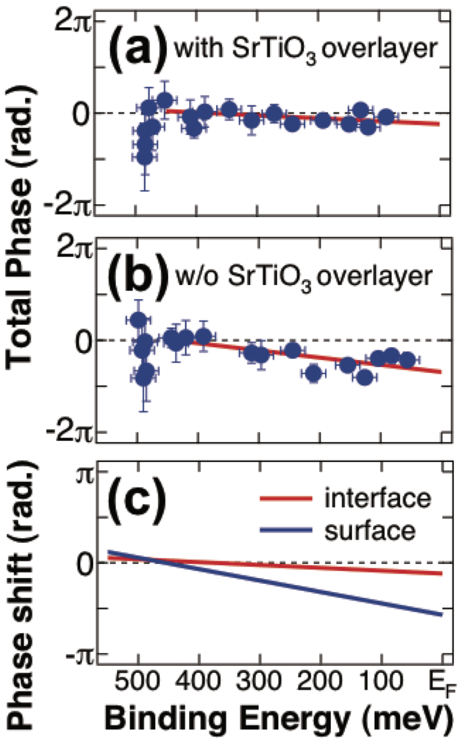

Fig. 6: Plots of the total phase shift of the metallic quantum well states in $SrVO_3$ layers (a) with and (b) without a $SrTiO_3$ overlayer as a function of binding energy. The markers with error bars denote the total phase shift obtained from analyzing the experimental data (see text for details). The solid lines are the results of the least-squares linear fitting for the data. (c) The phase shift at the $SrVO_3$ surface and the $SrTiO_3/SrVO_3$ interface.

reproduce the experimental results well, confirming that these observed states are derived from the quantized states in SVO layers in the metallic QW structures.

Figures 6(a) and 6(b) show the evaluated energy dependence of the total phase shifts in both QW structures. The experimentally obtained total phase shifts are well fitted by a least-squares regression line as indicated by the solid lines in Figs. 6(a) and 6(b). The slopes of the total phase shifts as a function of binding energy are considerably different between the two QW structures. The difference in the total phase shift is responsible for the modulation of the wave function in the QW at the boundaries. To examine the behavior of the standing waves at the boundaries of the SVO layers, we extracted the phase shifts at the surface and interface separately by solving the simple simultaneous equations (see Fig. 3). The separate phase shifts are shown in Fig. 6(c). As expected from the difference of total phase shifts in Figs. 6(a) and 6(b), the phase shift at the interface is almost independent of the binding energy and close to zero. On the contrary, the phase shift at the surface strongly depends on binding energy, and its absolute value is considerably higher than that at the interface from 500 meV to E_F where the QW states were observed from the ARPES spectra. The phase shift at the surface is farther from zero than that at the interface, indicating that the standing waves are considerably better confined at the interface than at the surface. In particular, nearly perfect reflection of standing waves is achieved at the STO/SVO interface. This result suggests that the interfaces with STO are useful for the quantum confinement of the V 3*d* states in SVO.

Finally, we briefly discuss the reason why an STO layer acts as a nearly ideal potential barrier in terms of the band diagram at the SVO/STO interface. The band diagrams drawn from previous photoemission studies [4,9] are illustrated in Fig. 7. At the interface between the metallic SVO and the *n*-type semiconductor STO, a Schottky potential barrier of 0.9 eV is formed. Because STO has a wide band gap of 3.2 eV, the occupied V 3*d* states involved in the formation of the observed QW states in the energy range from E_F to 0.5 eV are located around the middle of the band gap of STO. Namely, the occupied QW states are energetically well isolated from the conduction band minimum (offset of ~0.9 eV) and valence band maximum

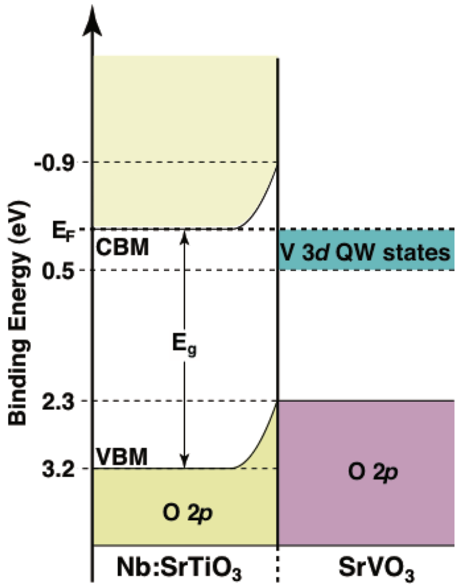

Fig. 7: Band diagram of the $SrTiO_3/SrVO_3$ interface deduced from the previous PES studies. CBM and VBM denote the conduction band minimum and valence band maximum, respectively. The V 3*d* conduction bands are energetically well isolated from both the CBM and VBM owing to the wide band gap of $SrTiO_3$ and its band lineup to $SrVO_3$.

(offset of ~1.8 eV) of STO at the interface. In such circumstances, it is difficult for an electron in the SVO layer to couple to any electronic states in STO.

Considering the band lineup at the SVO/STO interface in Fig. 7, the STO layers are regarded as a "vacuum" with higher permittivity for the V 3*d* electrons at a first approximation. STO is a quantum paraelectric material and its relative permittivity at the present measurement temperature of 20 K is more than 10,000 [10], although the value may degrade in thin film form and/or crystal deformation in the interfacial region [11]. At such a high value of permittivity, the barrier-energy lowering near the interface due to the image force (image-force lowering known as the Schottky effect) [12] is negligibly weak, and the shape of energy potential near the interface approaches asymptotically to the intrinsic Schottky barrier as shown in Fig. 7. In other words, an abrupt potential well is formed at the interface, and consequently nearly ideal quantum confinement of V 3*d* electrons could be achieved. These results have an important implication for designing oxide QW structures: other oxide semiconductors with a wide band gap and a high permittivity may be used as nearly ideal potential barriers to confine electrons in oxide heterostructures.

References

[1] T.-C. Chiang, Surf. Sci. Rep. **39**, 181 (2000).

[2] M. Milun, P. Pervan, and D. P. Woodruff, Rep. Prog. Phys. **65**, 99 (2002).

[3] N. V. Smith, N. B. Brookes, Y. Chang, and P. D. Johnson, Phys. Rev. B **49**, 332 (1994).

[4] K.Yoshimatsu, K.Horiba, H.Kumigashira, T. Yoshida, A. Fujimori, and M. Oshima, Science **333**, 319 (2011).

[5] A. F. Santander-Syro, O. Copie, T. Kondo, F. Fortuna, S. Pailhés, R. Weht, X. G. Qiu, F. Bertran, A. Nicolaou, A. Taleb-Ibrahimi, P. LeFévre, G. Herranz, M.Bibes, N.Reyren, Y. Apertet, P. Lecoeur, A. Barthélémy, and M. J. Rozenberg, Nature (London) **469**, 189 (2011).

[6] W. Meevasana, P. D. C. King, R. H. He, S-K. Mo, M. Hashimoto, A. Tamai, P. Songsiriritthigul, F. Baumberger, and Z-X. Shen, Nat. Mater. **10**, 114 (2011).

[7] P. D. C. King, R. H. He, T. Eknapakul, P. Buaphet, S.-K. Mo, Y. Kaneko, S. Harashima, Y. Hikita, M. S. Bahramy, C. Bell, Z. Hussain, Y. Tokura, Z.-X. Shen, H. Y. Hwang, F. Baumberger, and W. Meevasana, Phys. Rev. Lett. **108**, 117602 (2012)

[8] K. Yoshimatsu, E. Sakai, M. Kobayashi, K. Horiba, T. Yoshida, A. Fujimori, M. Oshima, and H. Kumigashira, *Phys. Rev. B* **88**, 115308 (2013).

[9] M. Minohara, I. Ohkubo, H. Kumigashira, and M. Oshima, Appl. Phys. Lett. **90**, 132123 (2007).

[10] K. A. Müller and H. Burkard, Phys. Rev. B **19**, 3593 (1979).

[11] A. A. Sirenko, C. Bernhard, A. Golnik, A. M. Ckark, J. Hao,W. Si, and X. X. Xi, Nature (London) **404**, 373 (2000).

[12] S. M. Sze and K. K. Ng, *Physics of Semiconductor Devices*, 3rd ed. (Wiley, Hoboken, NJ, 2007).